

Kinetic investigation of the planar Multipole Resonance Probe for arbitrary pressure

Chunjie Wang,¹ Michael Friedrichs,² Jens Oberrath,² and Ralf Peter Brinkmann¹

*¹Institute of Theoretical Electrical Engineering,
Ruhr University Bochum, D-44780 Bochum, Germany*

*²Department of Electrical Power Engineering,
South Westphalia University of Applied Science, 59494 Soest, Germany*

(Dated: May 16, 2022)

Abstract

Active plasma resonance spectroscopy (APRS) refers to a class of plasma diagnostic methods that use the ability of plasma to resonate at or near the electron plasma frequency for diagnostic purposes. The planar multipole resonance probe (pMRP) is an optimized realization of APRS. It has a non-invasive structure and allows simultaneous measurement of electron density, electron temperature, and electron-neutral collision frequency. Previous work has investigated the pMRP through the Drude model and collision-less kinetic model. The Drude model misses important kinetic effects such as collision-less kinetic damping. The collision-less kinetic model is able to capture pure kinetic effects. However, it is only applicable to the low-pressure plasma. To further study the behavior of the pMRP, we develop a collisional kinetic model in this paper, which applies to arbitrary pressure. In this model, the kinetic equation is coupled to the Poisson equation under the electrostatic approximation. The real part of the general admittance is calculated to describe the spectral response of the probe-plasma system. Both collision-less kinetic damping and collisional damping appear in the spectrum. This model provides a possibility to calculate the electron density, electron temperature, and electron-neutral collision frequency from the measurements.

Keywords: planar multipole resonance probe, kinetic effects, collision-less damping, collisional damping

I. INTRODUCTION

In the past decades, the industrial application of plasma technology has made remarkable progress [1, 2]. Plasma is used in many fields, such as etching, cleaning, and deposition. In the industrial process, plasma parameters, such as electron density and temperature, directly affect the quality of products. It is very important to accurately control plasma parameters throughout the process.

Precise control of plasma parameters depends on reliable diagnostic techniques. Representative measurement methods include the Langmuir probe [3, 4], optical emission spectroscopy [5, 6], and APRS probes [7–28]. APRS (active plasma resonance spectroscopy) refers to a class of plasma diagnostic methods that use the ability of plasma to resonate at or near the electron plasma frequency for diagnostic purposes [7, 8]. At present, APRS probes are considered as promising diagnostic methods. An attractive feature of APRS probes is that they are insensitive to additional dielectric deposition on the probe tip. The detailed advantages and disadvantages of APRS probes can be found in [9, 10].

Considering that the insertion of the probe can lead to plasma density depletion around the probe tip and its holder, non-invasive probes are preferred in the sensitive plasma process. In the past decade, several planar-type APRS probes have been developed, such as the planar multipole resonance probe (pMRP) [10–16], curling probe [17–19], and flat cutoff probe [20–22]. These probes can be flatly embedded into the chamber wall or chuck for minimally invasive process monitoring.

The pMRP is developed from the spherical multipole resonance probe (MRP) [23–26]. It consists of two semi-disc electrodes covered by a thin dielectric layer, which maintains a high degree of geometric and electrical symmetry. The pMRP allows simultaneous measurement of electron density, electron temperature, and electron-neutral collision frequency. It is a very promising non-invasive APRS probe.

To evaluate plasma parameters from the spectra detected by the probe, mathematical models are very important. In [7] (Drude model) and [8] (kinetic model), the generic properties of electrostatic APRS probes were investigated by the functional analytic approach. For any possible probe design, the spectral response function can be expressed as a matrix element of the resolvent of the dynamical operator. The Drude model is mathematically simple but physically limited. It only covers collisional damping. However, in the kinetic

spectral response, residual damping appears in the vanishing pressure limit. This collision-less damping can only be interpreted as kinetic effects, which have been verified in further studies [16, 26–28]. A brief comparison of the Drude model and kinetic model is shown in Tab. I.

TABLE I: Comparison of the Drude model and kinetic model

Drude model	Kinetic model
formulated in 3D space	formulated in 3D3V space
accessible to standard simulation tools	inaccessible to standard simulation tools
covers collisional damping	covers collision-less and collisional damping
yields electron density and collision frequency	yields electron density, temperature, and collision frequency

Previous work has studied the pMRP with the Drude model [10–16] and collision-less kinetic model [16]. The collision-less kinetic model ignores all collisions, and it only applies to the low-pressure plasma (a few Pa). By comparing the spectrum of the Drude model and collision-less kinetic model, we found that both models can provide an accurate resonance frequency for calculating the electron density from the measured spectrum. But the collision-less kinetic model also yields the electron temperature, which is not available in the Drude model. As predicted in [8], the kinetic spectrum is obviously broadened by collision-less kinetic damping. This damping is non-negligible and even plays a dominant role in the low-pressure plasma. However, the Drude model only includes collisional damping. This indicates that the collision frequency calculated by the Drude model is very inaccurate, especially in the low-pressure plasma. The collision-less kinetic model only covers collision-less kinetic damping. As the gas pressure increases, the collisional damping gets stronger, which cannot always be ignored.

In this paper, we will present a collisional kinetic model that applies to arbitrary pressure. It is able to cover collision-less kinetic damping and collisional damping. Obviously, due to the introduction of collisions, this model is mathematically more complex than the collision-less kinetic model. Next, we will take argon plasma as an example to introduce the collisional kinetic model and the corresponding kinetic spectra.

II. EQUILIBRIUM AND UNPERTURBED TRAJECTORY

As shown in Fig. 1, the idealized pMRP consists of two semi-disc electrodes. The electrodes are insulated from each other and from the grounded chamber wall. A thin dielectric layer with covers the electrodes and chamber wall. As described in [14, 16], we assume that the chamber wall is infinite and the insulator is ignorable. A naturally oriented Cartesian coordinate system (x, y, z) is used, which locates the dielectric at $-d < z < 0$ and the plasma at $z > 0$.

When the electrodes of the pMRP are grounded $\bar{\Phi}|_{E_{\pm}} = 0$, a static equilibrium appears in front of the dielectric layer. In the low-pressure plasma, this equilibrium behaves as a collision-less planar sheath [16], which follows the Bohm model [29]. To describe the static equilibrium at arbitrary pressure, a chemistry-free cold ion model is adopted: the equation of continuity expresses a constant ion flux $-\Psi_i$ towards the dielectric

$$n_i v_i = -\Psi_i, \quad (1)$$

and the equation of motion expresses the acceleration under the electric field \bar{E} and the collisional friction in the neutral gas background

$$m_i v_i \frac{\partial v_i}{\partial z} = e \bar{E} - \frac{\sqrt{v_T^2 + v_i^2}}{\lambda_i} m_i v_i \quad (2)$$

with the transition speed $v_T = 630$ m/s in argon. In terms of the friction force, we take an effective model that combines the regimes of constant collision frequency v_T/λ_i at low ion velocity and constant mean free path λ_i at high ion velocity [30]. Assuming a constant electron temperature T_e , the electron follows the Boltzmann relation

$$T_e \frac{\partial n_e}{\partial z} = -e n_e \bar{E}. \quad (3)$$

The Poisson equation relates the electric field to the charge density

$$\epsilon_0 \frac{\partial \bar{E}}{\partial z} = e(n_i - n_e) \quad (4)$$

with

$$\bar{E} = -\frac{\partial\bar{\Phi}}{\partial z}. \quad (5)$$

To write equations in dimensionless form, we use the following reference quantities: electron temperature T_e , density \hat{n} , electron plasma frequency $\hat{\omega}_{pe} = \sqrt{e^2\hat{n}/(m_e\epsilon_0)}$, Debye length $\hat{\lambda}_D = \sqrt{\epsilon_0 T_e/(e^2\hat{n})}$. The normalization follows: $z \rightarrow \hat{\lambda}_D z$, $t \rightarrow t/\hat{\omega}_{pe}$, $\bar{\Phi} \rightarrow (T_e/e)\bar{\Phi}$, $\bar{E} \rightarrow \sqrt{\hat{n}T_e/\epsilon_0}\bar{E}$, $n_i \rightarrow \hat{n}n_i$, $n_e \rightarrow \hat{n}n_e$, $v_i \rightarrow \sqrt{T_e/m_i}v_i$, $v_e \rightarrow \sqrt{T_e/m_e}v_e$, $\Psi_i \rightarrow \hat{n}\sqrt{T_e/m_i}\Psi_i$, $v_T \rightarrow \sqrt{T_e/m_i}v_T$, $\lambda_i \rightarrow \hat{\lambda}_D\lambda_i$. In dimensionless form, the sheath model reads

$$n_i v_i = -\Psi_i, \quad (6)$$

$$v_i \frac{\partial v_i}{\partial z} = \bar{E} - \frac{\sqrt{v_T^2 + v_i^2}}{\lambda_i} v_i, \quad (7)$$

$$\frac{\partial n_e}{\partial z} = -n_e \bar{E}, \quad (8)$$

$$\frac{\partial \bar{E}}{\partial z} = n_i - n_e, \quad (9)$$

$$\bar{E} = -\frac{\partial\bar{\Phi}}{\partial z}. \quad (10)$$

Fig. 2 depicts a floating sheath in an argon plasma at 10 Pa.

The motion of the electron under the static potential $\bar{\Phi}$ is defined as the unperturbed trajectory. In [16], the collision-less kinetic model is solved based on the unperturbed trajectory. This approach will also be adopted in this paper. As in [16], we introduce the coordinate system (ε_z, τ) based on the unperturbed trajectory. ε_z is the total energy of the electron in the z direction, and τ describes the corresponding temporal parametrization. A coordinate transformation is then defined as

$$(z, v_z) \begin{array}{c} \xrightarrow{\varepsilon_z = \mathcal{E}_z(z, v_z), \tau = \mathcal{T}(z, v_z)} \\ \xleftarrow{z = Z(\varepsilon_z, \tau), v_z = V_z(\varepsilon_z, \tau)} \end{array} (\varepsilon_z, \tau). \quad (11)$$

More detailed descriptions of the unperturbed trajectory, coordinate system (ε_z, τ) , and coordinate transformation $(z, v_z) \rightleftharpoons (\varepsilon_z, \tau)$ can be found in [16]. Here, we define a new

parameter

$$\varepsilon = \mathcal{E}(z, |\vec{v}|) = \frac{1}{2} |\vec{v}|^2 - \bar{\Phi}(z). \quad (12)$$

Both ε_z and ε remain constant on the unperturbed trajectory. These parameters and coordinate transformation will be used in later calculations.

III. KINETIC MODEL OF THE PROBE-PLASMA SYSTEM

A static planar sheath appears in front of the pMRP when its electrodes are grounded. During the measurement process, RF voltages are applied to the electrodes

$$\Phi|_{E_{\pm}} = \pm \hat{V} \cos(\omega t), \quad (13)$$

thereby generating a dynamic perturbation in the plasma around the probe. As described in [8], we assume that $\omega_{pe} \gtrsim \omega \gtrsim \nu \gg \nu_i \approx \omega_{pi} \gg \omega_g$ (elastic collision frequency ν , inelastic collision frequency ν_i , ion plasma frequency ω_{pi} , slow frequencies of all neutral gas phenomena ω_g). This assumption allows to focus only on the dominant collision: electron-neutral elastic collision. In the limit of $m_e/m_N \rightarrow 0$, the neutral particle is considered as an immobile scattering center, and it finally yields an angle and velocity independent differential collision frequency by assuming the hard-sphere collision. The electron distribution function $f(\vec{r}, \vec{v}, t)$ thus follows

$$\frac{\partial f}{\partial t} + \vec{v} \cdot \nabla_r f + \nabla \Phi \cdot \nabla_v f = \frac{\nu}{4\pi} \int_{\Omega} f(\vec{r}, |\vec{v}| \vec{e}, t) d\Omega - \nu f. \quad (14)$$

As in [14, 16], the potential follows the Poisson equation under the electrostatic approximation

$$-\nabla \cdot (\epsilon_r \nabla \Phi) = \begin{cases} 0 & \text{Dielectric} \\ n_i - \int f d^3v & \text{Plasma} \end{cases}, \quad (15)$$

with

$$\epsilon_r = \begin{cases} \epsilon_D & \text{Dielectric} \\ 1 & \text{Plasma} \end{cases}. \quad (16)$$

Under a small perturbation, the linear response theory applies [31, 32]: f and Φ can be split

into an equilibrium value and a small perturbation

$$f(\vec{r}, \vec{v}, t) = \bar{f}(z, \vec{v})(1 + \delta f(\vec{r}, \vec{v}, t)), \quad (17)$$

$$\Phi(\vec{r}, t) = \bar{\Phi}(z) + \delta\Phi(\vec{r}, t), \quad (18)$$

in which

$$\bar{f}(z, \vec{v}) = f_M(z, \vec{v}) = \frac{1}{(2\pi)^{3/2}} \exp\left(-\frac{1}{2}(v_x^2 + v_y^2 + v_z^2) + \bar{\Phi}(z)\right), \quad (19)$$

$$|\delta f| \ll 1, \quad (20)$$

$$|\delta\Phi| \ll |\bar{\Phi}|. \quad (21)$$

Substituting (17) and (18) into (14) and (15), the linearized equations read

$$\frac{\partial \delta f}{\partial t} + \vec{v} \cdot \nabla_r \delta f - \vec{v} \cdot \nabla \delta\Phi + \bar{\Phi}'(z) \frac{\partial \delta f}{\partial v_z} = \frac{\nu}{4\pi} \int_{\Omega} \delta f(\vec{r}, |\vec{v}| \vec{e}, t) d\Omega - \nu \delta f, \quad (22)$$

$$-\nabla \cdot (\epsilon_r \nabla \delta\Phi) = \begin{cases} 0 & \text{Dielectric} \\ -\int \bar{f} \delta f d^3v & \text{Plasma} \end{cases}. \quad (23)$$

As in [16], we assume that the perturbation terms are time-harmonic

$$\delta f(\vec{r}, \vec{v}, t) = \text{Re} \left[\delta \tilde{f}(\vec{r}, \vec{v}) \exp(i\omega t) \right], \quad (24)$$

$$\delta\Phi(\vec{r}, t) = \text{Re} \left[\delta \tilde{\Phi}(\vec{r}) \exp(i\omega t) \right]. \quad (25)$$

Since the equilibrium distribution is uniform in x and y , we apply the Fourier transform

$$\underline{\delta \tilde{f}}(k_x, k_y, z, \vec{v}) = \int_{-\infty}^{\infty} \int_{-\infty}^{\infty} \delta \tilde{f}(\vec{r}, \vec{v}) \exp(i(k_x x + k_y y)) dx dy, \quad (26)$$

$$\underline{\delta \tilde{\Phi}}(k_x, k_y, z) = \int_{-\infty}^{\infty} \int_{-\infty}^{\infty} \delta \tilde{\Phi}(\vec{r}) \exp(i(k_x x + k_y y)) dx dy. \quad (27)$$

Therefore, the partial derivatives in (22) and (23) are simplified

$$\frac{\partial}{\partial t} \rightarrow i\omega, \quad (28)$$

$$\frac{\partial}{\partial x} \rightarrow -ik_x, \quad (29)$$

$$\frac{\partial}{\partial y} \rightarrow -ik_y. \quad (30)$$

In the following calculations, k_x and k_y are temporarily omitted from $\delta\underline{f}$ and $\delta\underline{\Phi}$ before performing the inverse Fourier transform. Now, the linearized equations (22) and (23) become

$$\begin{aligned} & (\nu + i(\omega - k_x v_x - k_y v_y))\delta\underline{f} + v_z \frac{\partial \delta\underline{f}}{\partial z} + \bar{\Phi}'(z) \frac{\partial \delta\underline{f}}{\partial v_z} \\ & = -i(k_x v_x + k_y v_y)\delta\underline{\Phi} + v_z \frac{\partial \delta\underline{\Phi}}{\partial z} + \frac{\nu}{4\pi} \int_{\Omega} \delta\underline{f}(z, |\vec{v}| \vec{e}) d\Omega, \end{aligned} \quad (31)$$

$$(k_x^2 + k_y^2)\delta\underline{\Phi} - \frac{\partial^2 \delta\underline{\Phi}}{\partial z^2} = \begin{cases} 0 & \text{Dielectric} \\ -\int \bar{f} \delta\underline{f} d^3v & \text{Plasma} \end{cases}. \quad (32)$$

Due to the integral in the collision term, the kinetic equation (31) is very complicated. Hence, we define a new function

$$\delta\underline{g}(z, \varepsilon) = \frac{1}{4\pi} \int_{\Omega} \delta\underline{f}\left(z, \sqrt{2(\varepsilon + \bar{\Phi}(z))} \vec{e}\right) d\Omega, \quad (33)$$

so

$$\frac{1}{4\pi} \int_{\Omega} \delta\underline{f}(z, |\vec{v}| \vec{e}) d\Omega = \delta\underline{g}\left(z, \frac{1}{2}|\vec{v}|^2 - \bar{\Phi}(z)\right). \quad (34)$$

Substituting (34) into (31), and then transforming (z, v_z) into (ε_z, τ) , the kinetic equation is simplified into

$$\begin{aligned} & (\nu + i(\omega - k_x v_x - k_y v_y))\delta\underline{f}(Z(\varepsilon_z, \tau), v_x, v_y, V_z(\varepsilon_z, \tau)) + \frac{\partial \delta\underline{f}(Z(\varepsilon_z, \tau), v_x, v_y, V_z(\varepsilon_z, \tau))}{\partial \tau} \\ & = -i(k_x v_x + k_y v_y)\delta\underline{\Phi}(Z(\varepsilon_z, \tau)) + \frac{\partial \delta\underline{\Phi}(Z(\varepsilon_z, \tau))}{\partial \tau} + \nu \delta\underline{g}\left(Z(\varepsilon_z, \tau), \frac{1}{2}(v_x^2 + v_y^2) + \varepsilon_z\right). \end{aligned} \quad (35)$$

By integrating along the unperturbed trajectory, we get the solution of the kinetic equation

$$\begin{aligned} & \delta \underline{f}(Z(\varepsilon_z, \tau), v_x, v_y, V_z(\varepsilon_z, \tau)) \\ = & \delta \underline{\Phi}(Z(\varepsilon_z, \tau)) - (\nu + i\omega) \int_{-\infty}^{\tau} \exp((\nu + i(\omega - k_x v_x - k_y v_y))(\tau' - \tau)) \delta \underline{\Phi}(Z(\varepsilon_z, \tau')) d\tau', \quad (36) \\ & + \nu \int_{-\infty}^{\tau} \exp((\nu + i(\omega - k_x v_x - k_y v_y))(\tau' - \tau)) \delta \underline{g}(Z(\varepsilon_z, \tau'), \frac{1}{2}(v_x^2 + v_y^2) + \varepsilon_z) d\tau' \end{aligned}$$

where all the perturbation is accumulated along the unperturbed trajectory through the integral from $-\infty$ to τ .

Substituting (36) into (33) (Appendix A), the definition of $\delta \underline{g}(z, \varepsilon)$ yields

$$\delta \underline{g}(z, \varepsilon) - \delta \underline{\Phi}(z) = \int_0^{\infty} K_0(\nu + i\omega, k, z, z', \varepsilon) \left(\nu \delta \underline{g}(z', \varepsilon) - (\nu + i\omega) \delta \underline{\Phi}(z') \right) dz', \quad (37)$$

where $k = \sqrt{k_x^2 + k_y^2}$ and K_0 is related to the integral terms in (36). Substituting (36) into (32) (Appendix B), the Poisson equation becomes

$$k^2 \delta \underline{\Phi}(z) - \frac{\partial^2 \delta \underline{\Phi}(z)}{\partial z^2} = \begin{cases} 0 & \text{Dielectric} \\ - \exp(\bar{\Phi}(z)) \delta \underline{\Phi}(z) \\ + (\nu + i\omega) \int_0^{+\infty} K_1(\nu + i\omega, k, z, z') \delta \underline{\Phi}(z') dz' & \text{Plasma} \\ - \nu \int_{-\bar{\Phi}(z)}^{+\infty} \int_0^{+\infty} K_2(\nu + i\omega, k, z, z', \varepsilon) \delta \underline{g}(z', \varepsilon) dz' d\varepsilon \end{cases}, \quad (38)$$

where K_1 is related to the first integral term in (36) and K_2 is related to the second. When the electrodes of the pMRP are grounded, the equilibrium distribution only varies in the z direction. This uniformity on x and y is transferred to k_x and k_y in the Fourier space. Hence, $k = \sqrt{k_x^2 + k_y^2}$ finally appears in (37) and (38). In Fourier space, the boundary conditions

read

$$\delta\tilde{\Phi}(-d) = \hat{V} \iint_{E_{\pm}} \text{sign}(y) \exp(i(k_x x + k_y y)) dx dy, \quad (39)$$

$$\delta\tilde{\Phi}(0_-) = \delta\tilde{\Phi}(0_+), \quad (40)$$

$$\epsilon_D \delta\tilde{\Phi}'(0_-) = \delta\tilde{\Phi}'(0_+), \quad (41)$$

$$\delta\tilde{\Phi}(+\infty) = 0. \quad (42)$$

The definition of $\delta\tilde{g}(z, \varepsilon)$ (37) can be numerically discretized into a matrix equation that defines the relationship between $\delta\tilde{g}$ and $\delta\tilde{\Phi}$ at a certain ε . Substituting this matrix equation into (38) and then summing over all ε , the Poisson equation and the boundary conditions eventually yield a matrix equation for $\delta\tilde{\Phi}$, which gives the numerical solution of the potential. Afterwards, we can calculate the real part of the general complex admittance $\text{Re}[Y(\omega)]$, whose detailed derivation can be found in [16].

IV. SPECTRAL RESPONSE OF THE PROBE-PLASMA SYSTEM

In [16], we studied the idealized pMRP with a collision-less kinetic model. This model is able to capture the collision-less kinetic damping, which obviously broadens the spectrum of the idealized pMRP. This collision-less kinetic damping becomes stronger as the electron temperature increases. In this section, we will use the collisional kinetic model to further investigate the spectrum of the idealized pMRP with a focus on the effect of electron-neutral collisions on the kinetic spectrum. The same idealized pMRP as in [16] is chosen: electrode radius $R = 5$ mm, dielectric thickness $d = 0.04$ mm, dielectric relative permittivity $\epsilon_D = 4.82$. The kinetic spectra are calculated when this probe monitors an argon plasma as shown in Fig. 2.

Fig. 3 presents the kinetic spectra of the idealized pMRP, represented by the real part of its general complex admittance $\text{Re}[Y(\omega)]$. When the electron-neutral collision frequency $\nu = 0$, the spectral resonance and its broadening by pure kinetic effects are clearly visible. $\text{Re}[Y(\omega)]$ reaches a maximum value of 2.43 mS at $0.46 \hat{\omega}_{pe}$, and the half width of the resonance peak is $0.12 \hat{\omega}_{pe}$. As described in [8], the probe generates kinetic free energy. This energy can be transported by electrons from the probe to such a large distance that the probe cannot detect it. The loss of kinetic free energy will cause collision-less damping in the spectrum. When ν increases from 0 to $0.2 \hat{\omega}_{pe}$, the spectrum exhibits almost the same resonance frequency. But the resonance peak becomes lower and the half-width becomes higher (Fig. 4), which indicates the presence of stronger collisional damping. Now, we can conclude that this model is able to cover both collision-less damping and collisional damping.

The collisional kinetic model offers the possibility to calculate the electron density, electron temperature, and electron-neutral collision frequency from the measured spectrum. However, it's difficult to describe the relationship between the kinetic spectrum and plasma parameters with specific equations. One possible way is to build a spectral database from parameter studies at different n_e , T_e , and ν . By comparing the measured spectrum with the spectral database, the plasma parameters can be evaluated.

V. CONCLUSION AND OUTLOOK

To investigate the behavior of an idealized pMRP, we develop a collisional kinetic model which applies to arbitrary pressure. A static planar sheath appears in front of the pMRP when its electrodes are grounded. As the electrodes are applied with RF voltages, a dynamic perturbation will be generated around the probe. Under a small perturbation, the linearized kinetic model, including the kinetic equation and Poisson equation, is employed to study the kinetic spectral response of the probe-plasma system. Considering the planar geometry of the pMRP, we perform the Fourier transform in the directions parallel to the probe (x and y). The formulas are then derived and solved in Fourier space. This approach shows high superiority in planar geometry, and we can expect it to be applied to other planar-type APRS probes.

The spectral response of the idealized pMRP is expressed by the real part of the general complex admittance. When the electron-neutral collision frequency $\nu = 0$, the spectral resonance and its broadening by pure kinetic effects are clearly visible. As ν increases from 0 to $0.2\hat{\omega}_{pe}$, stronger collisional damping appears in the kinetic spectrum. This collisional kinetic model covers both collision-less kinetic damping and collisional damping. It yields the electron density, electron temperature, and electron-neutral collision frequency.

In [15], Friedrichs *et al* compared the pMRP spectra of analytic approach, electrostatic simulation, and electromagnetic simulation. They found that the main difference between the spectra of idealized pMRP and real pMRP is caused by the thickness of the insulator between the electrodes and the chamber wall. So far, our team has developed three analytic models: the Drude model [14], the collision-less kinetic model [16], and the collisional kinetic model (this paper). But all these analytic models are based on the idealized pMRP geometry. Therefore, further work is needed to optimize these analytic models by taking into account the influence of insulator thickness, which will bring certain challenges to the potential calculation.

VI. ACKNOWLEDGMENTS

The authors gratefully acknowledge the financial support by Deutsche Forschungsgemeinschaft (DFG) via the project DFG 360750908. Gratitude is expressed to the MRP-Team at Ruhr University Bochum.

References

- [1] Lieberman M A and Lichtenberg A J 2005 *Principles of Plasma Discharges and Materials Processing* 2nd edn (New York: Wiley)
- [2] Shul R J, Pearton S J *et al* 2011 *Handbook of advanced plasma processing techniques* (Springer Science & Business Media)
- [3] Merlino R L 2007 *Am. J. Phys.* **75** 1078
- [4] Godyak V A and Alexandrovich B M 2015 *J. Appl. Phys.* **118** 233302
- [5] Donnelly V M 2004 *J. Phys. D: Appl. Phys.* **37** R217
- [6] Zhu X-M and Pu Y-K 2010 *J. Phys. D: Appl. Phys.* **43** 403001
- [7] Lapke M, Oberrath J, Mussenbrock T and Brinkmann R P 2013 *Plasma Sources Sci. Technol.* **22** 025005
- [8] Oberrath J and Brinkmann R P 2014 *Plasma Sources Sci. Technol.* **23** 045006
- [9] Kim D W, You S J, Kim J H, Chang H Y, and Oh W Y 2016 *Plasma Sources Sci. Technol.* **25** 035026
- [10] Pohle D, Schulz C, Oberberg M, Awakowicz P and Rolfes I 202 *IEEE Trans. Microwave Theory Tech.* **68** 2067
- [11] Pohle D *et al* 2018 A stacked planar sensor concept for minimally invasive plasma monitoring 2018 Asia-Pacific Microwave Conference (APMC) 1315–7
- [12] Schulz C and Rolfes I 2014 A new approach on advanced compact plasma sensors for industrial plasma applications 2014 *IEEE Sensors Applications Symposium (SAS)* 263–266
- [13] Schulz C, Styrnoll T, Awakowicz P and Rolfes I 2014 *IEEE Trans. Instrum. Meas.* **64** 857
- [14] Friedrichs M and Oberrath J 2018 *EPJ Technol. Instrum.* **5** 7
- [15] Friedrichs M, Pohle D, Rolfes I and Oberrath J 2019 Planar Multipole Resonance Probe: Comparison of Full-wave Electromagnetic Simulation and Electrostatic Approximation 2019 *Kleinheubach Conference* 1-3
- [16] Wang C, Friedrichs M, Oberrath J and Brinkmann R P 2021 *Plasma Sources Sci. Technol.* **30** 105011
- [17] Pandey A, Sakakibara W, Matsuoka H, Nakamura K and Sugai H 2014 *Appl. Phys. Lett.* **104** 024111
- [18] Arshadi A, Brinkmann R P, Hotta M and Nakamura K 2017 *Plasma Sources Sci. Technol.* **26** 045013
- [19] Arshadi A and Brinkmann R P 2017 *Plasma Sources Sci. Technol.* **26** 015011
- [20] Kim D W, You S J, Kim S J, Kim J H, Lee J Y, Kang W S and Hur M 2019 *Plasma Sources Sci. Technol.* **28** 015004
- [21] Yeom H J, Kim J H, Choi D H, Choi E S, Yoon M Y, Seong D J, You S J and Lee H-C 2020 *Plasma Sources Sci. Technol.* **29** 035016
- [22] Yeom H J, You K H, Kim J-H and Lee H-C 2021 *Plasma Sources Sci. Technol.* **30** 065012

- [23] Lapke M, Mussenbrock T and Brinkmann R P 2008 *Appl. Phys. Lett.* **93** 051502
- [24] Oberrath J and Brinkmann R P 2014 *Plasma Sources Sci. Technol.* **23** 065025
- [25] Fiebrandt M, Oberberg M and Awakowicz P 2017 *J. Appl. Phys.* **122** 013302
- [26] Oberrath J 2020 *Plasma Sources Sci. Technol.* **29** 055005
- [27] Oberrath J and Brinkmann R P 2016 *Plasma Sources Sci. Technol.* **25** 065020
- [28] Oberrath J 2018 *Plasma Sources Sci. Technol.* **27** 045003
- [29] Bohm D 1949 *The Characteristics of Electrical Discharges in Magnetic fields* ed A Guthrie and R K Wakerling (New York: McGraw–Hill)
- [30] Hornbeck J A 1951 *Phys. Rev.* **84** 615
- [31] Krall N A and Trivelpiece A W 1973 *Principles of plasma physics* (New York: McGraw–Hill)
- [32] Buckley R 1966 *Proc. R. Soc. Lond. A* **290** 18

VII. APPENDIX A. DEFINITION OF $\underline{\delta\tilde{g}}(z, \varepsilon)$

Defining

$$\delta\tilde{h}(z, \varepsilon) = \nu\delta\underline{\tilde{g}}(z, \varepsilon) - (\nu + i\omega)\delta\tilde{\Phi}(z), \quad (\text{A.1})$$

the solution of kinetic equation (36) reads

$$\begin{aligned} \delta\underline{\tilde{f}}(Z(\varepsilon_z, \tau), v_x, v_y, V_z(\varepsilon_z, \tau)) &= \delta\tilde{\Phi}(Z(\varepsilon_z, \tau)) \\ + \int_{-\infty}^{\tau} \exp((\nu + i(\omega - k_x v_x - k_y v_y))(\tau' - \tau)) \delta\underline{\tilde{h}}\left(Z(\varepsilon_z, \tau'), \frac{1}{2}(v_x^2 + v_y^2) + \varepsilon_z\right) d\tau'. \end{aligned} \quad (\text{A.2})$$

Defining

$$\tau_+ = \mathcal{T}\left(z, \sqrt{2(\varepsilon_z + \bar{\Phi}(z))}\right), \quad (\text{A.3})$$

$$\tau_- = \mathcal{T}\left(z, -\sqrt{2(\varepsilon_z + \bar{\Phi}(z))}\right), \quad (\text{A.4})$$

and then substituting (A.2) into the definition of $\underline{\delta\tilde{g}}(z, \varepsilon)$ (33), the first part gives

$$\frac{1}{4\pi} \int_{\Omega} \int_0^{+\infty} \delta\tilde{\Phi}(Z(\varepsilon_z, \tau)) \delta(Z(\varepsilon_z, \tau) - z) dZ d\Omega = \delta\tilde{\Phi}(z), \quad (\text{A.5})$$

and the second part gives

$$\begin{aligned}
& \frac{1}{4\pi} \int_{\Omega} \int_0^{+\infty} \int_0^{+\infty} \int_{-\infty}^{\tau} \exp((\nu + i(\omega - k_x v_x - k_y v_y))(\tau' - \tau)) \\
& \delta \tilde{h} \left(Z(\varepsilon_z, \tau'), \frac{1}{2}(v_x^2 + v_y^2) + \varepsilon_z \right) \delta(Z(\varepsilon_z, \tau) - z) \\
& \delta \left(\sqrt{v_x^2 + v_y^2 + 2(\varepsilon_z + \bar{\Phi}(z))} - \sqrt{2(\varepsilon + \bar{\Phi}(z))} \right) d\tau' dZ dV d\Omega \\
& = \frac{1}{4\sqrt{\varepsilon + \bar{\Phi}(z)}} \int_0^{\sqrt{2(\varepsilon + \bar{\Phi}(z))}} \int_{-\bar{\Phi}(z)}^{\varepsilon} \frac{1}{\sqrt{\varepsilon_z + \bar{\Phi}(z)}} \int_{-\infty}^{+\infty} \int_{-\infty}^{\tau} \exp((\nu + i\omega)(\tau' - \tau)) \\
& J_0(kv_{xy}(\tau' - \tau)) \delta \tilde{h} \left(Z(\varepsilon_z, \tau'), \frac{1}{2}v_{xy}^2 + \varepsilon_z \right) (\delta(\tau - \tau_+) + \delta(\tau - \tau_-)) \\
& \delta(v_{xy} - \sqrt{2(\varepsilon - \varepsilon_z)}) d\tau' d\tau d\varepsilon_z dv_{xy} \\
& = \frac{1}{4\sqrt{\varepsilon + \bar{\Phi}(z)}} \int_{-\bar{\Phi}(z)}^{\varepsilon} \frac{1}{\sqrt{\varepsilon_z + \bar{\Phi}(z)}} \\
& \left(\int_{-\infty}^{\tau_+} \exp((\nu + i\omega)(\tau' - \tau_+)) J_0(k\sqrt{2(\varepsilon - \varepsilon_z)}(\tau' - \tau_+)) \delta \tilde{h}(Z(\varepsilon_z, \tau'), \varepsilon) d\tau' \right. \\
& \left. + \int_{-\infty}^{\tau_-} \exp((\nu + i\omega)(\tau' - \tau_-)) J_0(k\sqrt{2(\varepsilon - \varepsilon_z)}(\tau' - \tau_-)) \delta \tilde{h}(Z(\varepsilon_z, \tau'), \varepsilon) d\tau' \right) d\varepsilon_z
\end{aligned} \tag{A.6}$$

Since $d\tau' = dz' / \sqrt{2(\varepsilon_z + \bar{\Phi}(z))}$, the definition of $\delta \tilde{g}(z, \varepsilon)$ finally yields (37).

VIII. APPENDIX B. POISSON EQUATION

Substituting the solution of kinetic equation (36) into $\int \bar{f} \delta \tilde{f} d^3v$, the first part gives

$$\begin{aligned} & \int_{-\infty}^{+\infty} \int_{-\infty}^{+\infty} \int_{-\infty}^{+\infty} \int_0^{+\infty} \frac{1}{(2\pi)^{3/2}} \exp\left(-\frac{1}{2}(v_x^2 + v_y^2 + v_z^2) + \bar{\Phi}(z)\right) \delta \tilde{\Phi}(Z(\varepsilon_z, \tau)) \\ & \delta(Z(\varepsilon_z, \tau) - z) dZ dv_x dv_y dv_z \\ & = \exp(\bar{\Phi}(z)) \delta \tilde{\Phi}(z) \end{aligned} \quad , \quad (\text{B.1})$$

the second part gives

$$\begin{aligned} & -(\nu + i\omega) \int_{-\infty}^{+\infty} \int_{-\infty}^{+\infty} \int_{-\infty}^{+\infty} \int_0^{+\infty} \int_{-\infty}^{\tau} \frac{1}{(2\pi)^{3/2}} \exp\left(-\frac{1}{2}(v_x^2 + v_y^2 + v_z^2) + \bar{\Phi}(z)\right) \\ & \exp((\nu + i(\omega - k_x v_x - k_y v_y))(\tau' - \tau)) \delta \tilde{\Phi}(Z(\varepsilon_z, \tau')) \delta(Z(\varepsilon_z, \tau) - z) d\tau' dZ dv_x dv_y dv_z \\ & = -(\nu + i\omega) \int_{-\bar{\Phi}(z)}^{+\infty} \frac{\exp(-\varepsilon_z)}{2\sqrt{\pi}(\varepsilon_z + \bar{\Phi}(z))} \int_{-\infty}^{+\infty} \int_{-\infty}^{\tau} \exp\left((\nu + i\omega)(\tau' - \tau) - \frac{k^2(\tau' - \tau)^2}{2}\right) \\ & \delta \tilde{\Phi}(Z(\varepsilon_z, \tau')) (\delta(\tau - \tau_+) + \delta(\tau - \tau_-)) d\tau' d\tau d\varepsilon_z \\ & = -(\nu + i\omega) \int_{-\bar{\Phi}(z)}^{+\infty} \frac{\exp(-\varepsilon_z)}{2\sqrt{\pi}(\varepsilon_z + \bar{\Phi}(z))} \left(\int_{-\infty}^{\tau_+} \exp\left((\nu + i\omega)(\tau' - \tau_+) - \frac{k^2(\tau' - \tau_+)^2}{2}\right) \right. \\ & \left. \delta \tilde{\Phi}(Z(\varepsilon_z, \tau')) d\tau' + \int_{-\infty}^{\tau_-} \exp\left((\nu + i\omega)(\tau' - \tau_-) - \frac{k^2(\tau' - \tau_-)^2}{2}\right) \delta \tilde{\Phi}(Z(\varepsilon_z, \tau')) d\tau' \right) d\varepsilon_z \end{aligned} \quad , \quad (\text{B.2})$$

and the third part gives

$$\begin{aligned}
& \nu \int_{-\infty}^{+\infty} \int_{-\infty}^{+\infty} \int_{-\infty}^{+\infty} \int_0^{+\infty} \int_{-\infty}^{\tau} \frac{1}{(2\pi)^{3/2}} \exp\left(-\frac{1}{2}(v_x^2 + v_y^2 + v_z^2) + \bar{\Phi}(z)\right) \\
& \exp\left((\nu + i(\omega - k_x v_x - k_y v_y))(\tau' - \tau)\right) \delta_{\underline{g}}\left(Z(\varepsilon_z, \tau'), \frac{1}{2}(v_x^2 + v_y^2) + \varepsilon_z\right) \delta(Z(\varepsilon_z, \tau) - z) \\
& d\tau' dZ dv_x dv_y dv_z \\
= & \nu \int_{-\bar{\Phi}(z)}^{+\infty} \int_{-\bar{\Phi}(z)}^{\varepsilon} \frac{\exp(-\varepsilon)}{2\sqrt{\pi}(\varepsilon_z + \bar{\Phi}(z))} \\
& \left(\int_{-\infty}^{\tau_+} \exp((\nu + i\omega)(\tau' - \tau_+)) J_0\left(k\sqrt{2(\varepsilon - \varepsilon_z)}(\tau' - \tau_+)\right) \delta_{\underline{g}}(Z(\varepsilon_z, \tau'), \varepsilon) d\tau' \right. \\
& \left. + \int_{-\infty}^{\tau_-} \exp((\nu + i\omega)(\tau' - \tau_-)) J_0\left(k\sqrt{2(\varepsilon - \varepsilon_z)}(\tau' - \tau_-)\right) \delta_{\underline{g}}(Z(\varepsilon_z, \tau'), \varepsilon) d\tau' \right) d\varepsilon_z d\varepsilon
\end{aligned} \tag{B.3}$$

Since $d\tau' = dz'/\sqrt{2(\varepsilon_z + \bar{\Phi}(z))}$, the Poisson equation finally yields (38).

Figures

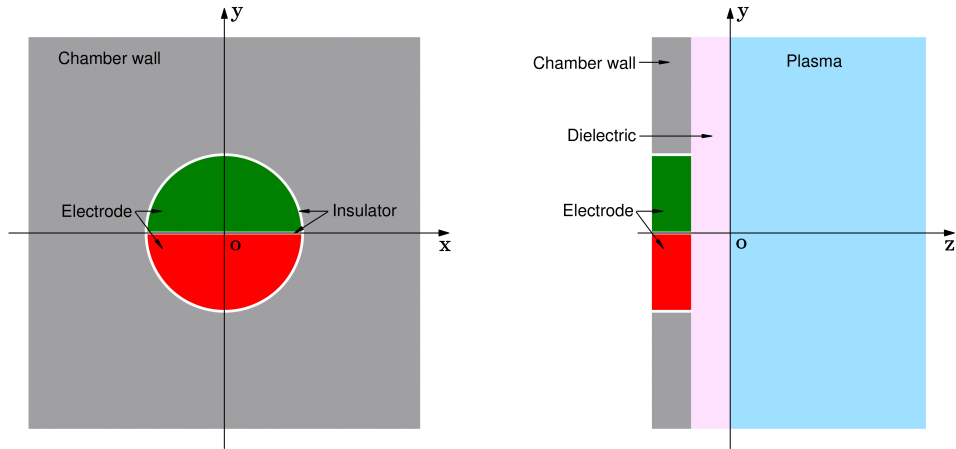


FIG. 1: Idealized planar Multipole Resonance Probe. Two semi-disc electrodes E_{\pm} with a radius of R are flatly integrated into the chamber wall. The electrodes are insulated from each other and from the grounded chamber wall. A thin dielectric layer with a thickness of d covers the electrodes and the chamber wall.

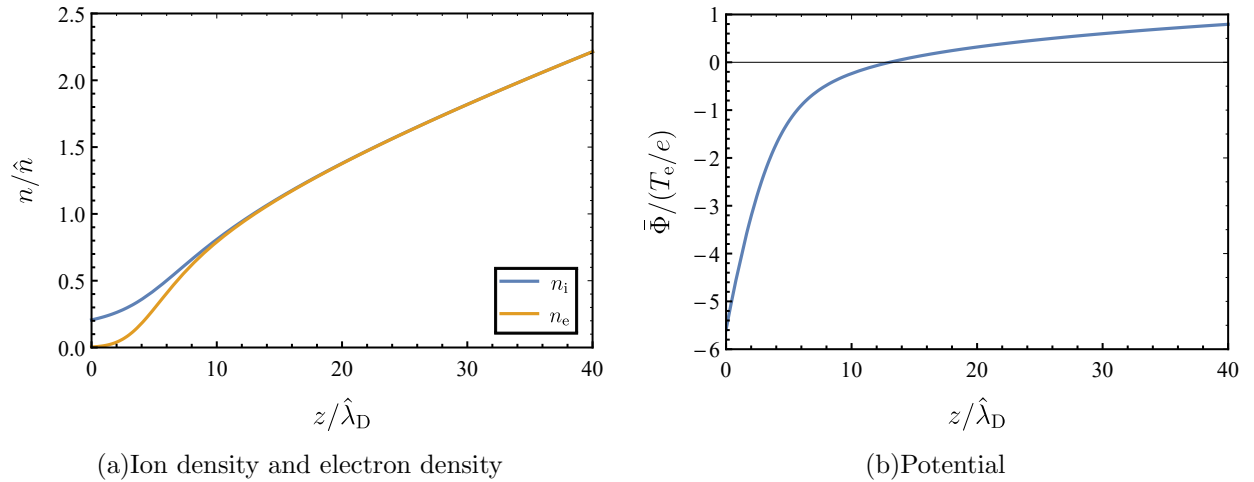


FIG. 2: Equilibrium distribution in an argon plasma at 10 Pa: $T_e = 2 \text{ eV}$, $\hat{n} = 10^{16} \text{ m}^{-3}$, $\hat{\lambda}_D = 0.11 \text{ mm}$.

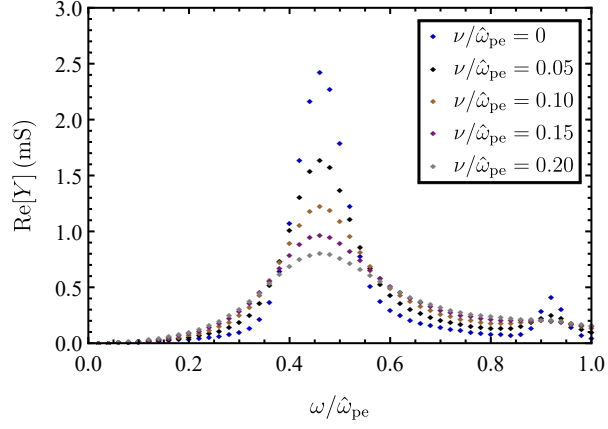


FIG. 3: Kinetic spectra of the idealized pMRP for different collision frequencies: $\hat{\omega}_{pe} = 5.64$ GHz.

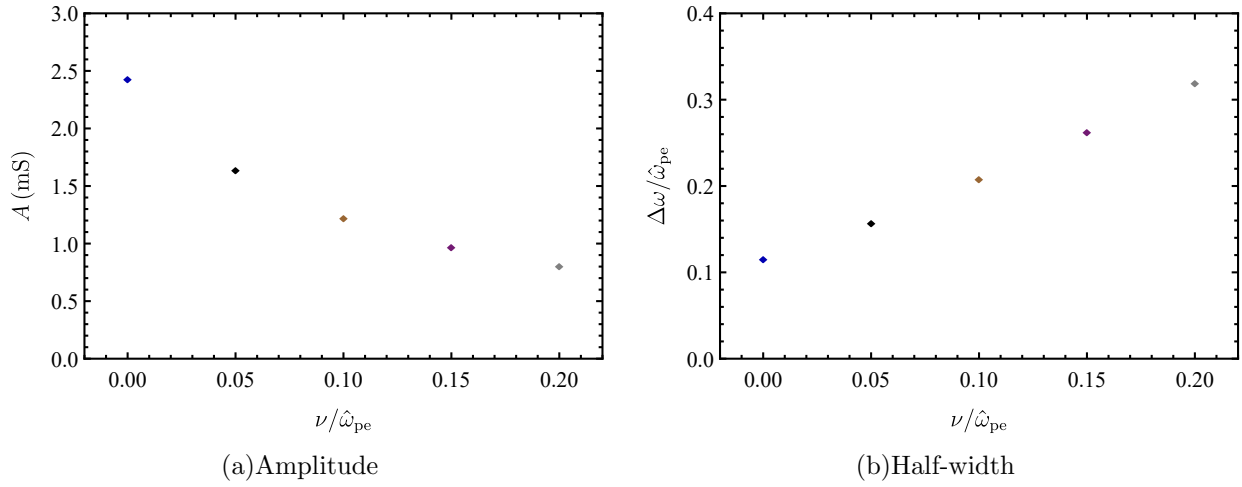


FIG. 4: Kinetic spectra of the idealized pMRP dependent on the collision frequency: $\hat{\omega}_{pe} = 5.64$ GHz.